Article

Graphene Oxide-Functionalized Bacterial Cellulose−Gelatin Hydrogel with Curcumin Release and Kinetics: In Vitro Biological Evaluation

Muhammad Umar Aslam Khan,* Goran M. Stojanović, Roselinda Ab Rehman,* Ali-Reza Moradi, Muhammad Rizwan, Nureddin Ashammakhi, and Anwarul Hasan*

Read Online

ACCESS | Metrics & More | Article Recommendations

ABSTRACT: Biopolymer-based bioactive hydrogels are excellent wound dressing materials for wound healing applications. They have excellent properties, including hydrophilicity, tunable mechanical and morphological properties, controllable functionality, biodegradability, and desirable biocompatibility. The bioactive hydrogels were fabricated from bacterial cellulose (BC), gelatin, and graphene oxide (GO). The GO-functionalized-BC (GO-*f*-BC) was synthesized by a hydrothermal method and chemically crosslinked with bacterial cellulose and gelatin using tetraethyl orthosilicate (TEOS) as a crosslinker. The structural, morphological, and wettability properties were studied using Fourier transform infrared spectroscopy (FTIR), scanning electron microscopy (SEM), and a universal testing machine (UTM), respectively. The swelling analysis was conducted in different media, and aqueous medium exhibited maximum hydrogel swelling compared to other media. The Franz diffusion method was used to study curcumin (Cur) release (Max = 69.32%, Min = 49.32%), and Cur release kinetics followed the Hixson−Crowell model. Fibroblast (3T3) cell lines were employed to determine the cell viability and proliferation to bioactive hydrogels. Antibacterial activities of bioactive hydrogels were evaluated against infection-causing bacterial strains. Bioactive hydrogels are hemocompatible due to their less than 0.5% hemolysis against fresh human blood. The results show that bioactive hydrogels can be potential wound dressing materials for wound healing applications.
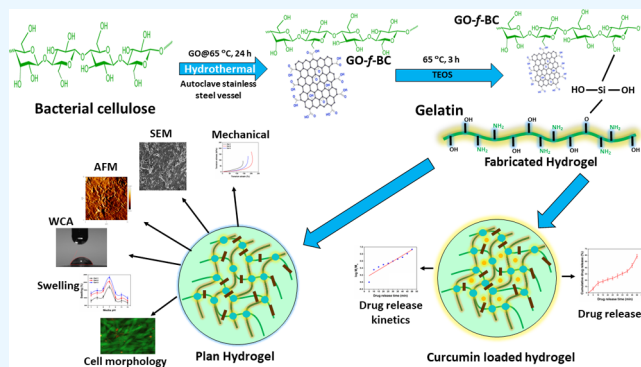
1. INTRODUCTION

Human skin defends the body from physical and environmental harmful effects and bacterial infections. The body may suffer from a skin wound if not appropriately treated until complete wound healing.[1,2] The biopolymer-based wound dressing is famous due to tissue remodeling, granulation, revascularization, and re-epithelialization that promote wound healing. Biopolymers have revolutionized medical science by designing and engineering advanced biomaterials with optimized applications.[3,4] The hydrogels fabricated from biopolymers have similar properties as natural extracellular matrices (ECMs). These hydrogels are ideal, as they possessed biocompatible, self-adhesive, and hemocompatible properties. They have multibiofunction properties, including improved antibacterial activity, cell viability, and proliferation, that support wound healing.[5,6] The controllable swelling and degradation are critical physicochemical characteristics of the wound dressing. The swelling behavior of hydrogels supports wound exudate management and controlled release of therapeutic agents. The swelling leads to biodegradation that facilitates burst release of therapeutic agents to protect the wound site from pathogens. Physicochemical stimuli can trigger the release of therapeutic agents, including pH, crosslinking, solvent composition, temperature, pressure, and electromagnetic stimuli.[7,8] Biochemical stimuli such as pH and ion concentration play a particular role in biochemical interactions, and these translational shifts can be reversed as triggers are removed. However, parameters such as monomer type, electron density, attached chains, and crosslinking density are fundamental factors that stimulate hydrogels.[9,10]

Cellulose is the most abundant plant-based biopolymer and has numerous biomedical applications. Acetic acid-producing bacterial species synthesize bacterial cellulose (BC) and have promising applications in hydrogel fabrication due to control-

lable physicochemical properties essential for nutrient and waste exchange.[11] Hydrogels have three-dimensional (3D) structures, and their inherent soft tissue-like properties with distinct physicochemical behavior promote cellular proliferation to promote wound healing.[12−14] Gelatin is a natural polymer and received attention in biomedical engineering because of its biocompatible, cell supporting properties for wound healing. It is a denatured form of collagen and an ideal biomaterial due to excellent biodegradable, antibacterial, and hemocompatible properties.[15,16] Gelatin-based hydrogels promote cell adherence, viability, and proliferation due to providing additional binding and active sites that accelerate wound healing. These limitations can be overcome by functionalizing or developing hybrid materials with other biopolymers.[17,18]

Graphene is a two-dimensional (2D) material, and graphene oxide (GO) with an excellent material has several promising applications. Its remarkable features, high surface area, available functional groups, conductive activity, and sp2 hybridization make it an exceptional biomedical engineering material.[2,19] Due to the variety of functional groups (hydroxyl and carboxyl), GO can be incorporated into polymeric matrices and influences the physicochemical properties. The improved physicochemical properties provide additional bonding and active sites and might interact with cell membranes via hydrogen bonding that supports cell adherence. The increased cell adhesion promotes cell viability and proliferation, facilitating wound healing by regulating other biofunctions.[20] Curcumin is a well-known natural medicine with several properties, such as antioxidative, anti-inflammatory, antimicrobial, and antitumor activities. It has low water solubilization and low bioavailability.[21] Curcumin (Cur) is poorly absorbed, and very little enters the bloodstream because of rapid physiological degradation.[22,23]

In this study, we have fabricated novel hydrogels from biopolymers (BC, gelatin) and GO by tetraethyl orthosilicate (TEOS) crosslinking. GO-f-BC was synthesized by a hydrothermal method and chemically crosslinked with BC and gelatin using TEOS to fabricate bioactive hydrogels. Fourier transform infrared spectroscopy (FTIR), scanning electron microscopy (SEM), and a universal testing machine (UTM) were employed to characterize hydrogel samples. The swelling in different media (aqueous, phosphate buffer saline (PBS)), electrolyte (sodium chloride (NaCl)) was studied at different pH scales at 37 °C. A water contact meter was used to evaluate the hydrophilicity and hydrophobicity of the hydrogels. The Franz diffusion method was used to study Cur release, and different mathematical models were studied to determine the Cur release mechanism. The biological studies used fibroblast (3T3) cell lines to evaluate cell viability and proliferation. The antibacterial activities were characterized using Gram (+ive and −ive) bacterial strains. In vitro, hemocompatibility assay was studied against fresh blood. The fabricated bioactive hydrogels would be promising for wound healing in biomedical applications.

2. MATERIALS AND METHODS

2.1. Chemical Materials. Bacterial cellulose was extracted by a well-reported method by Abba et al.[24] Gelatin (CAS # G9382-500G), tetraethyl orthosilicate (CAS # 78-10-4), phosphate buffer saline (PBS), sodium chloride (NaCl), absolute ethanol, and glacial acetic acid were supplied by Sigma Aldrich.

2.2. Biological Materials. The fibroblast (3T3) cell lines were supplied by American Type Culture Collection (ATCC). Fetal bovine serum (FBS), antibiotic (streptomycin/penicillin solution) containing Dulbecco's modified Eagle medium (DMEM), and live/dead cell staining were supplied by Gibco and Molecular Probes, respectively. There are two components in live/dead assay: component-A as calcein-AM (green) and component-B as BOBO-3 iodide (red).

2.3. Methods. *2.3.1. Fabrication of Hydrogels.* The polymeric composite system was prepared using BC and GO via a hydrothermal process, as summarized in Table 1. Briefly,

Table 1. Detailed Hydrogel Composition

hydrogel	bacterial cellulose (BC) g	graphene oxide (GO) mg	bacterial cellulose (BC) g	gelatin g	crosslinker (TEOS) μL
HGel-1	0.7	0	0.3	0	240
HGel-2	1.5	0.03	0.3	0.3	240
HGel-3	1.5	0.03	0	0.3	240

a homogeneous suspension of BC (1.5 g) and GO (0.03 mg) was prepared in 25 mL of deionized water and transferred into a stainless-steel autoclave vessel. It was kept in an oven for 24 h at 65 °C to get a graphene oxide-functionalized bacterial cellulose polymeric system. It was raised to 50 mL by adding deionized water. A gelatin suspension was made in 10 mL of deionized water by adding 0.3 g in the powder form and stirred with the polymeric system for 1 h at 60 °C to get a homogenized polymeric mixture. The crosslinker (TEOS) was added (240 μL dissolved in ethanol at 5 mL) and stirred at 60 °C for 2 h, as summarized in Table 1. After 2 h, potassium persulfate was added to initiate crosslinking and allowed to stir at conditions for 3 h; the proposed chemical interaction is shown in Figure 1. The bioactive hydrogels were transferred to a Petri dish and placed in an oven overnight at 55 °C. After 24 h, the dried films were carefully peeled off and packed for characterizations. These bioactive hydrogels were also filled in 24-well plates and covered with paraffin tape. Small holes were made in the paraffin tape using a spatula and kept at −40 °C for 24 h. The 24-well plates were kept in the freeze-drying compartment to get freeze-dried porous hydrogels. The hydrogel solutions were packed in airtight glass vials for biological assays. The codes were assigned to the fabricated hydrogels with regard to different formulations, such as HGel-1 = BC−BC, HGel-2 = GO-f-BC-BC, and HGel-3 = GO-f-BC-Gel, and the proposed chemical interaction is presented in Figure 2a.

2.3.2. Drug Loading. Curcumin was taken as a model drug to study its release and release kinetics. Briefly, CUR (25 mg) was dissolved in methanol (10 mL) and dropwise added to HGel-1, HGel-2, and HGel-3. These were stirred for 1 h at 60, and TEOS (240 μL) was added and stirred at 60 °C for 2 h. Then, it was crosslinked by adding potassium persulfate to start crosslinking, and stirring was continued at 60 °C for 3 h. The fabricated hydrogels were poured into Petri dishes after 3 h and placed in an oven at 55 °C to get well-dried hydrogels; the proposed chemical drug loading and interaction with the polymeric matrix of the hydrogel are illustrated in Figure 2b.

3. CHARACTERIZATIONS

The structure−functional groups and other structural behavior of the properties of the bioactive hydrogels were studied using
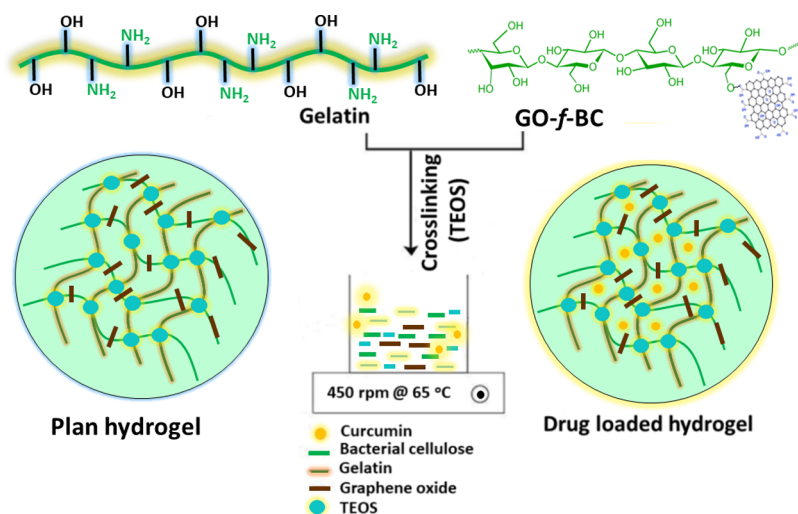
Figure 1. Schematic illustration presenting the fabrication of hydrogels from their essential components (bacterial cellulose, gelatin, graphene oxide, and TEOS) through simple blending. It illustrates the curcumin loading in the polymeric matrix of the hydrogel.
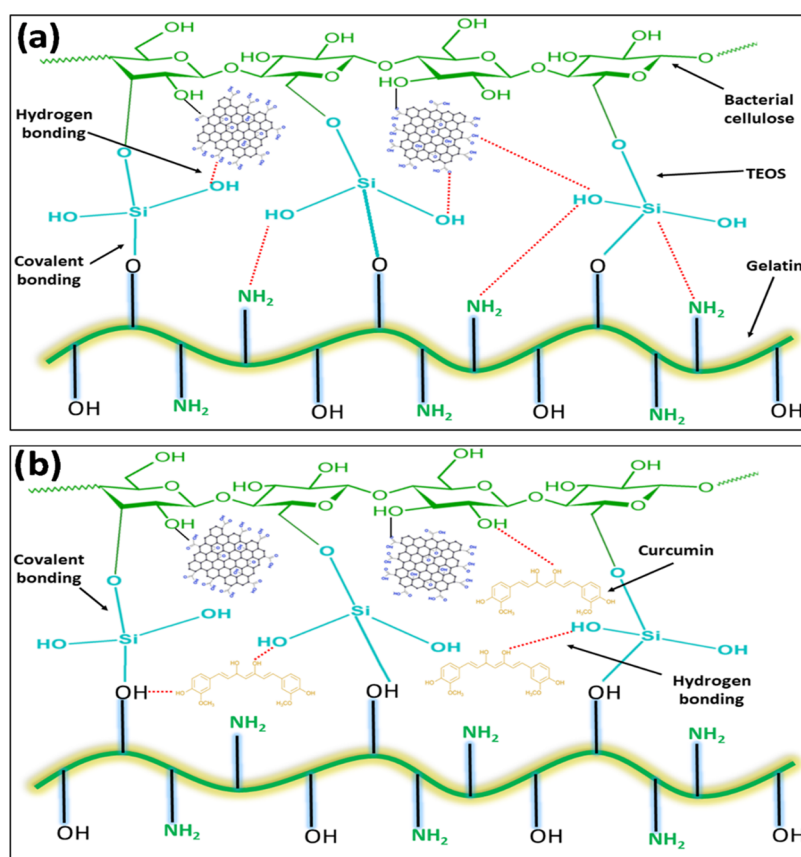

Figure 2. Proposed chemical interaction of the fabricated hydrogels: (a) proposed chemical interaction presents the crosslinking of graphene oxide-functionalized bacterial cellulose with gelatin through TEOS crosslinking and (b) curcumin loaded into the polymeric matrix of the hydrogel.

Fourier transform infrared spectroscopy (Nicolet 6700, Waltham, Massachusetts). The FTIR spectral profile was captured in the spectral region of 4000−600 cm^{-1}. The surface morphology of the hydrogels was studied using a scanning electron microscope (JEOL-JSM 5410 LV). The well-dried hydrogel samples were gold-sputtered, and SEM was operated under accelerated 10 kV voltage. The surface roughness of the well-dried hydrogel samples was determined by atomic force microscopy (AFM) (Park System XE-100). The double-sided

tape was used to immobilize 1 mm-thick hydrogel samples over the sample to perform surface roughness analysis. The wetting properties of bioactive hydrogels were examined via a water contact meter system (JY-82, Dingsheng, Chengde, China) to determine the hydrophobic and hydrophilic behavior.

3.1. Swelling Analysis. Swelling of any biomaterial, an essential phenomenon in tissue engineering, was examined at 37 °C for 24 h in different medium pH ranges. The bioactive hydrogels were cut into squares (50 mg) and placed in
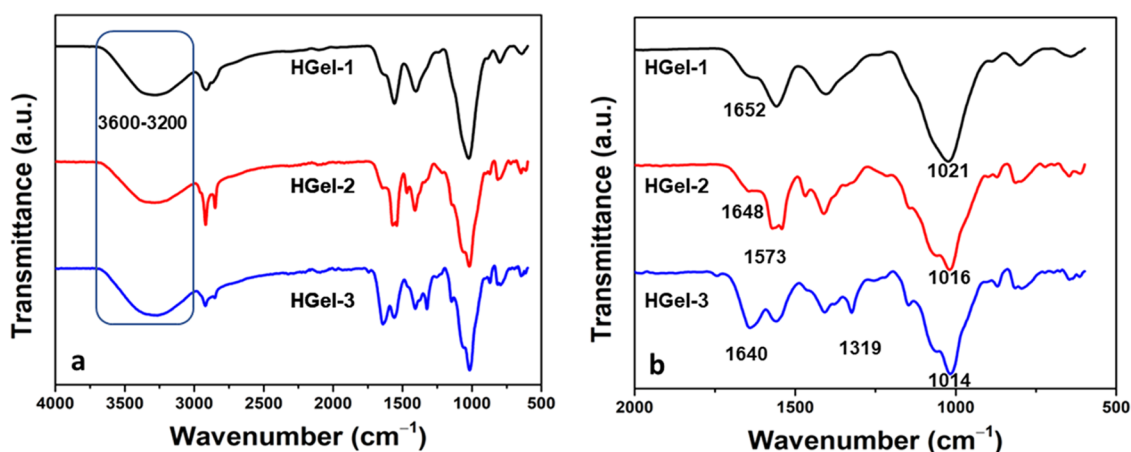
Figure 3. FTIR spectral profile of the hydrogels to determine their structural and different available functional groups: (a) spectral profile of the hydrogels ranging from 4000 to 500 cm^{-1} and (b) spectral profile of the hydrogels ranging from 2000 to 500 cm^{-1}.

different media (such as aqueous, PBS, and NaCl) with different pH values, and the 2 M concentration solution of NaCl was prepared. After a specific time, it was removed, and any excess surface water was gently wiped away using tissue paper. The weight of the swollen hydrogel samples was noted, and the swelling percentage was calculated using the equation following eq 1

$$\text{swelling } (\%) = \frac{W_f - W_i}{W_i} \times 100 \tag{1}$$

where W_i = initial weight and W_f = final weight.

3.2. Drug Release Analysis and Release Kinetics. The Franz diffusion method examined the controlled and sustained drug release in PBS media with a pH of 7.4. Briefly, a 2 mL sample of PBS media was run in a double-beam UV−vis spectrophotometer to analyze it. However, PBS medium was taken as a reference, and a standard curve was used to analyze drug release. The drug release kinetics was studied against zero-order, first-order, Hixson−Crowell, Korsmeyer−Peppas, Higuchi, and Baker−Lonsdale models, as shown in eqs 2−7.[25] The drug release kinetics were examined using drug release information from Franz diffusion at pH 7.4.

$$\text{zero} - \text{order} \quad M_t = M_o + K_o t \tag{2}$$

$$\text{first order } \log C = \log C_o - \frac{kt}{2.303} \tag{3}$$

$$\text{Higuchi model} \quad ft = Q = K_H \times t^{1/2} \tag{4}$$

$$\text{Hixson Crowell model} \quad W^{1/3} - W^{1/3} = kt \tag{5}$$

$$\text{Korsmeyer} - \text{Peppas model } \ln \frac{M_t}{M_o} = n \ln t + \ln K \tag{6}$$

Baker − Lonsdale model

$$F_t = \frac{2}{3}\left[1 - \left(1 - \frac{M_t}{M_o}\right)^{2/3}\right]\frac{M_t}{M_o} = K(t)^{0.5} \tag{7}$$

where K, K_o, and K_H = constants and M_t = drug release amount at "t" time.

3.3. In Vitro Assay. *3.3.1. Cell Viability and Proliferation.* Cell viability and proliferation of fibroblast cell lines were evaluated against the different dilutions (1.5, 2.0, 2.5, and 3.0

mg/mL) of bioactive hydrogels after various intervals (24, 48, and 72 h). The wells of the cell culture plates were coated with gelatin (0.1%), taken as the positive control. The cells were cultured in the plates, and these cell culture plates were incubated under standard in vitro conditions (5% CO$_2$, 95% humidity at 37 °C) for 2 h with neutral red (NR) medium. These were washed with PBS solution and treated with destaining media for 10 min to remove NR media. A microplate reader (ELx-800) (BioTek, Winooski, Vermont) was employed to evaluate the optical density, and cell viability was calculated using eq 8

$$\text{cell viability } (\%) = \frac{OD_s}{OD_c} \times 100 \tag{8}$$

where OD_s = optical density of the sample and OD_c = optical density of the positive control.

3.3.2. Cell Morphology. The fibroblast cell morphology was studied via live/dead assay to determine the cellular behavior against hydrogels. UV was used to sterilize the hydrogel samples for 5 min, and cells were seeded on hydrogel samples approximately with a density of 2×10^4 cells/hydrogel sample. The cells were maintained in 24-well plates, FBS (10%), and antibiotic (streptomycin/penicillin solution)-containing DMEM to culture cells. The hydrogel was seeded with fibroblast cell lines and incubated at different intervals (24, 48, and 72 h) under standard in vitro conditions (5% CO$_2$ at 37 °C). After different intervals, live/dead cell staining was performed as per the manufacturer's protocols to observe the hydrogel samples' cytocompatible and morphological behavior. Both live/dead assay kit components (Invitrogen R37601) were mixed, and 50 μL was added to the cell culture wells and incubated for 30 min at 37 °C in a CO$_2$ incubator. A fluorescent microscope (Olympus, FV300) was used to record the cell morphology.

3.3.3. Antibacterial Activities. The antibacterial behavior of hydrogels was studied against different Gram-(positive and negative) bacterial strains (*Escherichia coli*, *Pseudomonas aeruginosa*, and *Staphylococcus aureus*). The antibacterial behavior of the bioactive hydrogel was studied by the disk diffusion method, and antibacterial activities were studied via zone inhibition. Briefly, molten agar was poured into Petri dishes and allowed to solidify. A cotton swab was used to spread different bacterial strains (aforementioned) over the solidified agar. The well was made, and a micropipette was
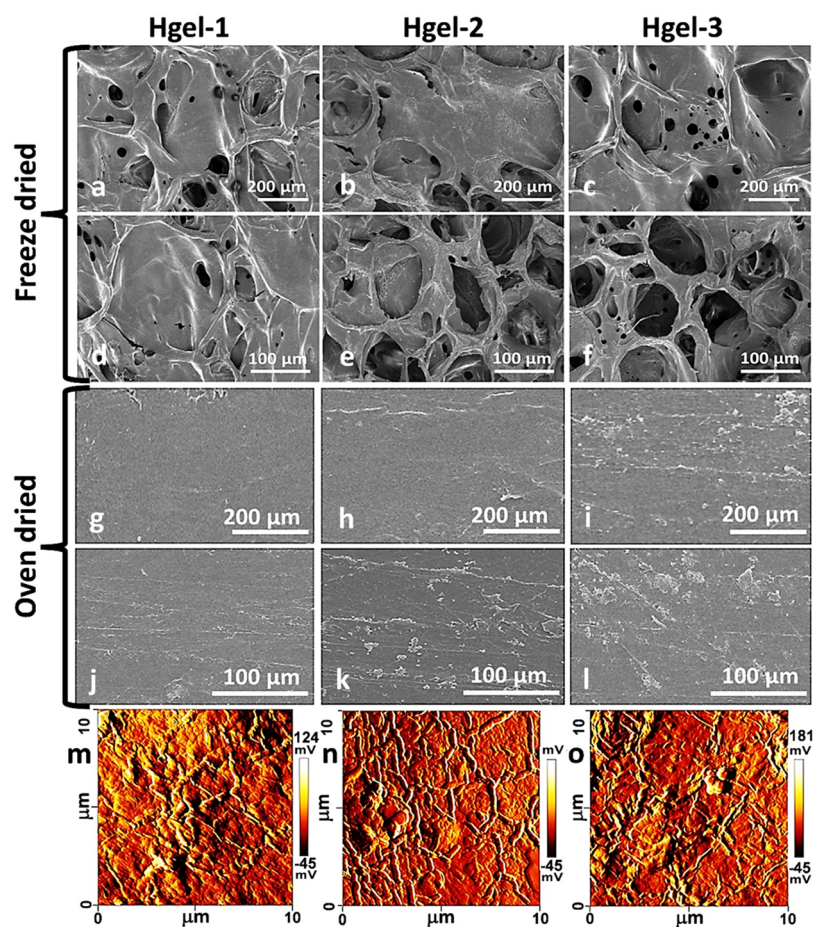
Figure 4. Surface morphology of the freeze-dried and oven-dried hydrogels: The surface morphology of the freeze-dried hydrogels (a−f) and oven dried hydrogels (g−l) was analyzed by SEM (200 and 100 μm) to evaluate the surface behavior of the fabricated hydrogels. AFM showing the surface roughness of the oven-dried hydrogels (m−o).

used to drop 75 μL of bioactive hydrogel into the well. These samples were incubated at 37 °C for 12 h in an oven, and antibacterial activities were studied by the zone inhibition (mm) method.

3.3.4. Hemocompatibility Analysis. The hemocompatibility assay was performed against fresh human blood supplied by the trauma center of a local hospital in Johor Bahru, Malaysia. The Ethics Committee approved the hemocompatibility assay obtained under UTM/2016/KHAIRUL NADWA/28-JAN./ 729-FEB-2016-JAN-2019. Blood was centrifuged at 500×/5 min, and different dilutions of bioactive hydrogels were prepared in PBS solution (pH 7.4 @ 37 °C). The samples of bioactive hydrogels were incubated at 37 °C with Triton (1%) and centrifuged at 1500×/5 min. A UV−vis spectrophotometer (UV−visible (HACH D500), Loveland, Colorado) was used to analyze the absorbance at λ = 540 nm, and the hemolysis percentage was calculated by eq 9

$$\text{hemolysis (\%)} = \frac{\text{Abs}_S - \text{Abs}_{NC}}{\text{Abs}_{PC} - \text{Abs}_{NC}} \times 100 \qquad (9)$$

where Abs_s = sample absorbance, Abs_{PC} = positive control absorbance, and Abs_{NC} = negative control absorbance.

3.4. Statistical Analysis. Statistical analysis of research data was studied using statistical software (IBM, SPSS Statistics 21) except for the morphological and structural studies. The standard errors (S.Es.) were presented in the figures as Y-error bars. With post hoc multiple comparisons,

two-way ANOVA was used. (*$p < 0.05$ and ***$p < 0.001$ size of the sample n = 3).

4. RESULTS AND DISCUSSION

4.1. Structural Analysis. The spectral profile of the bioactive hydrogels presents the different functional groups and peak positions. Figure 3 presents the spectral structure of the hydrogels to determine the structural and functional groups with their characteristics and band positions. The broadband region from 3600 to 3200 cm^{-1} was attributed to hydrogen bonding due to the available −OH functional groups of GO, TEOS, gelatin, and bacteria, confirming the intra/ interhydrogen bonding.[26] The peak positions at 1147 and 1064 cm^{-1} may be due to the C−O stretching of pyranose and O− H, confirming the successful crosslinking of BC and gel via TEOS. The absorption peaks at 2918 and 2851 cm^{-1} are due to the stretching vibration of −CH, and their intensity increased from HGel-1 to HGel-2. HGel-3 was compromised due to gelatin crosslinking. The asymmetric stretching of −Si− O−C and −Si−O−Si from 1110 to 1000 cm^{-1} was attributed to the TEOS crosslink.[27] This evidence confirms the successful crosslinking of the BC and gelatin. The peaks at 1739 and 1640 cm^{-1} are assigned to −C═C and −C═O stretching vibrations, respectively. These vibration peaks are due to GO and are only slightly visible in HGel-2 and HGel-3.[28] Hence, these vibrational peaks with the corresponding positions confirm the successful fabrication of hydrogels.
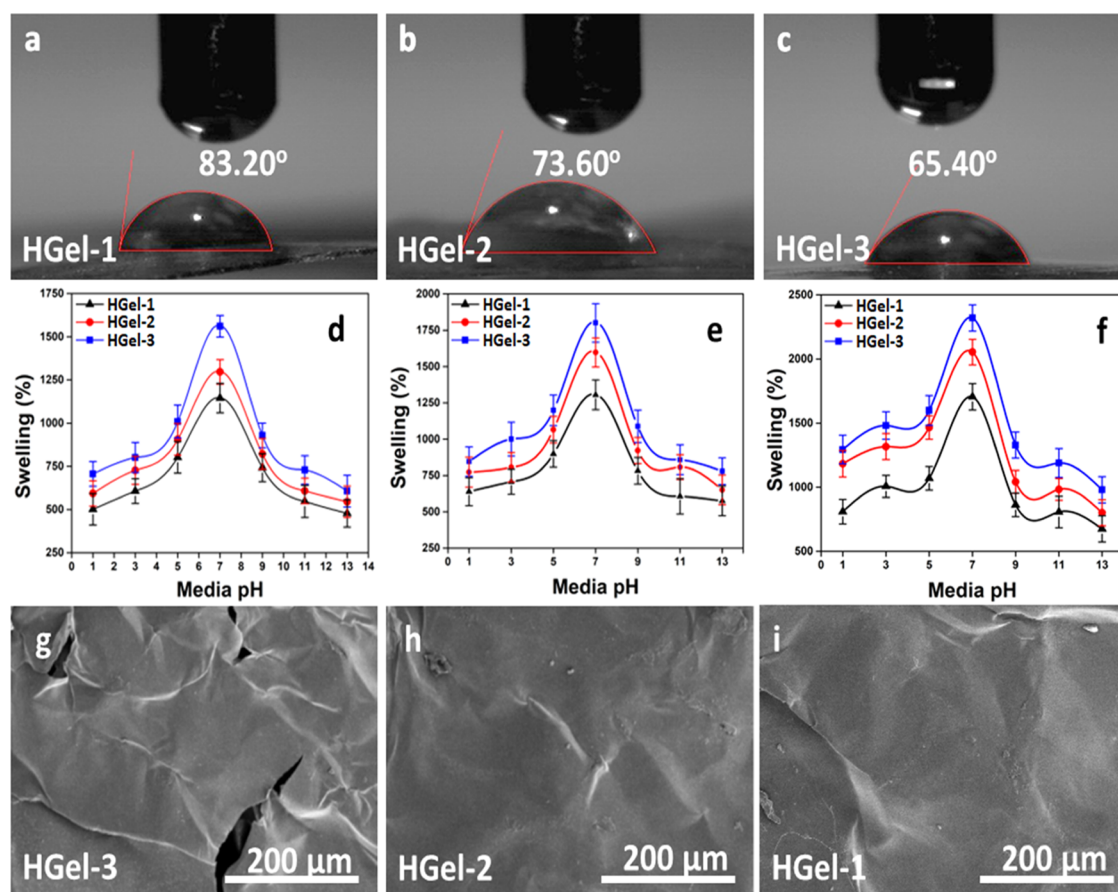
Figure 5. Physicochemical behavior of bioactive hydrogels: The wetting analysis of the hydrogel (a–c). The swelling behaviour in different media (d–f). The surface morphology of hydrogels was studied by SEM for surface behavior after 24 h of swelling in aqueous media (7.4 pH) at 37 °C in different media (g– i).

4.2. Surface Morphology. The SEM micrographs of the bioactive hydrogel are shown in Figure 4a−l, and each exhibit unique and different morphology due to different compositions and formulations. The freeze-dried hydrogels' morphology was highly porous, as shown in Figure 4a−f. The porous morphology with uniform pore distributions confirms the successful crosslinking of the bioactive hydrogels. These bioactive hydrogels have different morphologies and pore distributions due to different formulations.[29,30] The surface morphology of the oven-dried hydrogel films was also investigated at different magnifications (200 and 100 μm) to observe the surface behavior of hydrogels, as shown in Figure 4g−l. The bioactive hydrogel sample (HGel-1) has a smoother or less abrasive morphology as it does not contain GO. However, due to GO incorporation into the polymeric chains, hydrogel samples (HGel-2 and HGel-3) have uneven and rough morphology. Both hydrogels have a uniform GO flake distribution as macro/microislands, which would be due to the gradual drying rate of hydrogels and also the suspension homogeneity. These GO flakes can be either micro or macro in size, providing uneven or rough surfaces that offer extra active or binding sites for cell adherence to promote cellular activities. Such morphologies are essential for various biomedical applications, including drug delivery, tissue engineering, wound healing, etc.[30−32] Surface morphology is crucial for biomedical applications, particularly wound dressing. These SEM micrographs have proved that changing the method can fabricate hydrogels with different morphologies. Hence,

morphological analysis confirms that changing fabrication methods can fabricate hydrogels with different morphologies. It also confirms that the fabricated hydrogels have successful crosslinking and GO incorporation.

4.3. Surface Topography. Atomic force microscopy is an efficient tool for studying bioactive hydrogels' surface topography. The 2D surface roughness of the oven-dried bioactive hydrogel films is shown in Figure 4m−o. The polymeric matrix of the biopolymer (BC and gelatin) also can be observed by surface roughness. Moreover, GO plays an important role in GO-incorporated hydrogels and is also interpreted for topographical changes of hydrogel samples (HGel-2 and HGel-3). The results demonstrate that GO-functionalized hydrogels have a rough surface area than that without GO-functionalized (GHel-1). The GO-functionalized hydrogels may provide additional active or binding sites due to their rough topography and offer better cellular activities, including cell adherence that facilitates cell proliferation and viability.[33] The GO-cluster or GO-functionalized hydrogel has been marked with blue circles, and the results confirmed that HGel-2 and HGel-3 hydrogels present more rough topography than that of HGel-1.

4.4. Wetting Behavior. The wetting behavior of a biomaterial is a critical phenomenon and surface property that helps observe hydrophilic and hydrophobic behaviors. It also describes the interaction between the material and biological systems while contacting with biofluid. The wetting property is tunable and promotes cellular interaction with the

optimized surface of biomaterials. The biomaterial with hydrophilic behavior promotes cellular activities that promote wound healing.[11,34] As shown in Figure 5a−c, the wetting behavior of oven-dried hydrogels was characterized. It was observed that GO-incorporated hydrogels have more hydrophilicity at 0 seconds compared to hydrogels (HGel-1) without any GO contents. Since GO has several available hydrophilic functional groups, including −OH, it is also intriguing to learn that HGel-3 is more hydrophilic than HGel-2, as it has gelatin with excessive hydrophilic functional groups. The increasing hydrophilic nature of HGel-3 may be attributed to GO and gelatin. It may affect other parameters, including stiffness, swellability, surface charge, and swellability, which may impact biomedical applications.[35] These might also impact how cells react to the biomaterial during and after implantation, which would be advantageous for cell adhesion and growth.

4.5. Swelling Behavior in Different Media. The swelling of oven-dried hydrogels has been observed in different media, including aqueous (deionized water), PBS, and electrolyte (NaCl), in different pH levels at room temperature. Figure 5d−f illustrates the swelling of the bioactive hydrogels in various media and exhibits multiple behaviors depending on the pH of the media. To evaluate the surface morphology of well-dried hydrogels after 24 h of swelling in aqueous media, Figure 5g−i shows morphological phenomena. It was found that these hydrogels swelled most in aqueous media at pH 7 (neutral pH) than in acidic and basic media. It was observed that these bioactive hydrogels swelled more in acidic medium than at basic pH. Similar swelling behavior of hydrogels has been seen in PBS and NaCl but bioactive hydrogel swelling is more significant in PBS medium than in NaCl medium. The swelling trend can be observed in all hydrogels at aqueous > PBS > NaCl, under similar conditions. Additionally, it was found that the bioactive hydrogels containing graphene oxide swell more due to water interacting with the −OH functional groups. Since GO has several −OH and other hydrophilic functional groups, these functional groups tend to interact with water due to enhanced hydrogen bonding. More hydrogel swelling results from excessive hydrogen bonding.[36] The significant swelling behavior also helps absorb excessive wound exudate and blood from spilled containers because inadequate wound exudate can result in a bacterial attack, sometimes resulting in chronic illness and limb loss.[37] Moreover, significant hydrogel swelling at various pH levels may be essential in the sustained release of therapeutic agents that have been entrapped in the hydrogels. As a result, the fabricated bioactive hydrogels have a significant capacity to absorb biofluids and would thus be potential biomaterials with the desired properties for applications in wound healing.

4.6. Drug Release Assay. The sustained and controlled drug release from the polymeric matrix of the hydrogel is always challenging due to its complex releasing mechanism. It has four fundamental parameters to control drug releases: diffusion, solvent, degradation, erosion, and swelling.[38,39] In the erosion mechanism, drug delivery occurs due to a hydrolytic process, and the polymeric matrix of hydrogels begins to degrade at the edges and margins to release the drug.[40] Diffusion mechanisms release drugs from the hydrogel polymeric matrix when there is a concentration difference. The swelling of hydrogels is directly related to diffusion that interacts with body fluids and swells by absorbing biofluids to release the drug.[41] The size of the polymeric mesh increases when the hydrogel is applied to the injury site, swelling occurs

due to biofluid absorption, and diffusion occurs. The hydrogels interact with the biofluids, dissolve in them, and diffuse out from the polymeric matrix of the hydrogel. The trapped drug is released from the polymeric matrix and is available at the surface.[42] The maximum drug delivery occurs in HGel-1 at 7.4 pH in PBS media at 37 °C, even though all hydrogel samples have been loaded with a model drug (curcumin) with varying drug release percentages. However, under the same circumstances, as shown in Figure 6, HGel-3 delivers drugs at a lower
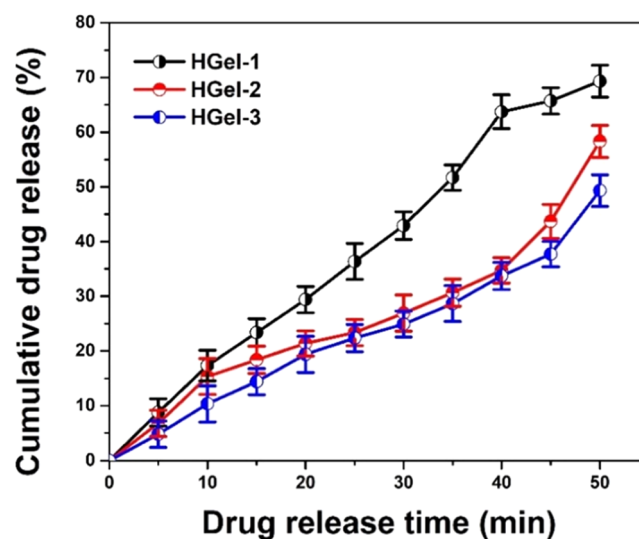

Figure 6. Cumulative drug release analysis of the hydrogels in PBS media at 37 °C.

rate compared to HGel-2. The drug release of HGel-1 has been consistent, with 40% drug release occurring after 40 min. HGel-2 has a different drug release mechanism compared to HGel-1; after 40 min, it has a sustained release of about 33% of the drug. Due to the crosslinking behavior of GO in HGel-2 and HGel-3, HGel-3 has the most delayed or sustained release, as it has ≈ 35%. Hydrogen bonding or weak attraction forces may be used by the drug to interact.

4.7. Drug Release Kinetics. The drug release kinetics of CUR has been studied using different mathematical models to determine the release mechanism shown in Figure 7a−r with numerical values summarized in Table 2. Several vital factors control the drug release from the polymeric matrix, such as chemical interaction type, drug loading mechanism, carrier nature, porosity, and carrier stimulus response.[43] Due to their different structures and compositions, these bioactive hydrogels possessed variable regression coefficient values (R^2). HGel-1 has a maximum R^2 value for Hixson−Crowell (0.97597) and a minimum R^2 value (0.53864) by Baker−Lonsdale. Similarly, HGel-2 and HGel-3 have maximum R^2 values (0.97597 and 0.99073, respectively). Both follow the drug release pathway, i.e., fitting the model Hixson−Crowell cube law and minimum value for R^2 (0.44273 and 0.66217) by fitting the same Hixson−Crowell model. Hence, these fabricated hydrogels best fit the Hixson−Crowell model with maximum R^2 values for HGel-1 = 0.97597, HGel-2 = 0.97597, and HGel-3 = 0.99073 following the drug release mechanism from a system having a change in surface area and diameter.[43]

4.8. Cell Morphology, Viability, and Proliferation. The cellular behavior (cell morphology, viability, and proliferation) was studied to evaluate the biocompatibility of hydrogels that
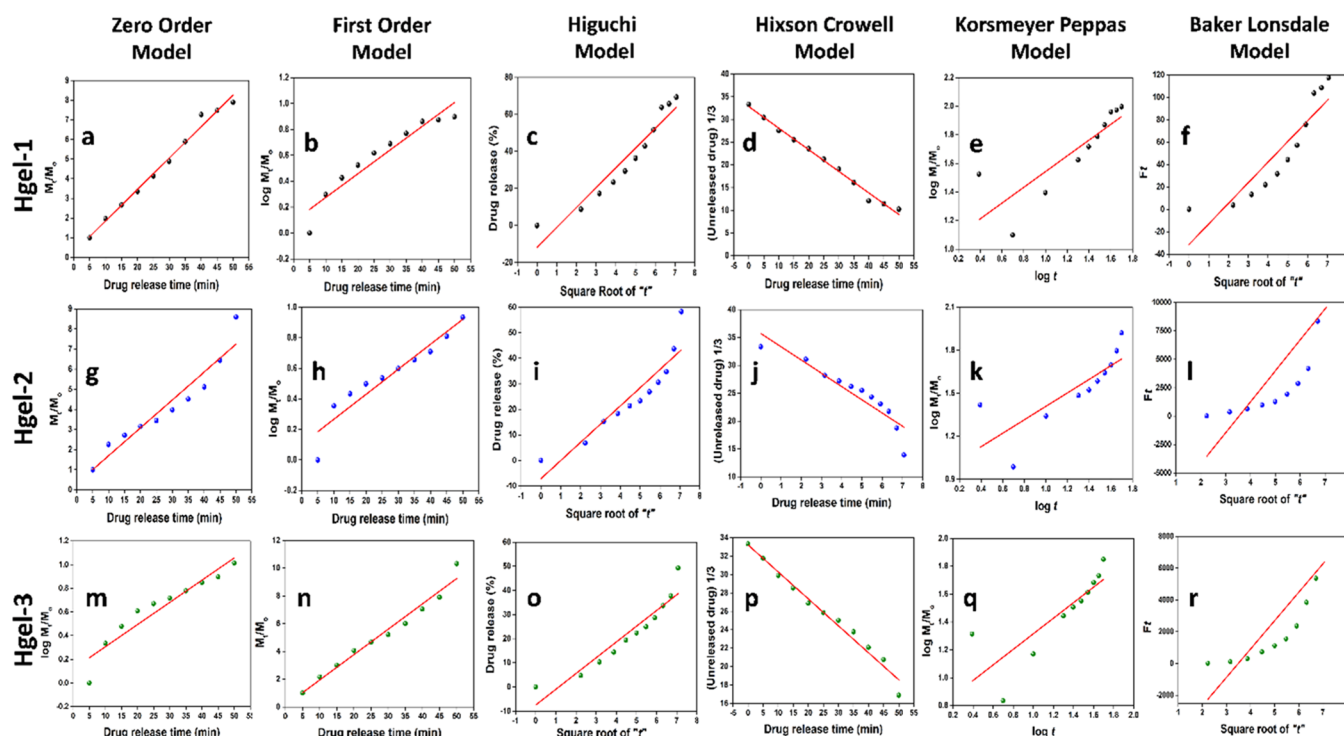
Figure 7. Drug release kinetics against various mathematical (zero-order (a, g, m), first-order (b, h, n), Higuchi (c, i, o), Hixson−Crowell (d, j, p), Korsmeyer−Peppas (e, k, q), and Baker−Lonsdale (f, l, r)) models against all hydrogel samples to determine the drug release behavior.

Table 2. Drug Release Kinetics of Hydrogels Have Been Summarized against Mathematical Models

sample	model type	intercept	slope	R^2
HGel-1	zero-order	0.12008	0.18248	0.96757
	first-order	0.11910	0.01875	0.88831
	Higuchi	−7.46373	6.52283	0.88356
	Hixson−Crowell	33.20288	−0.29249	0.97597
	Korsmeyer−Peppas	0.78581	0.55742	0.63479
	Baker−Lonsdale	−6234.3475	1787.44127	0.53864
HGel-2	zero-order	0.31082	0.13866	0.90661
	first-order	0.10291	0.01637	0.8928
	Higuchi	−7.12432	7.12524	0.84068
	Hixson−Crowell	35.70808	−2.37508	0.97597
	Korsmeyer−Peppas	0.93972	0.47027	0.58696
	Baker−Lonsdale	−9637.35993	2723.96978	0.44273
HGel-3	zero-order	0.2552	0.15995	0.98809
	first-order	0.09168	0.01832	0.90285
	Higuchi	−11.68647	10.69177	0.91633
	Hixson−Crowell	32.82409	−0.47492	0.99073
	Korsmeyer−Peppas	0.99183	0.55048	0.66217
	Baker−Lonsdale	−31.34229	18.36442	0.80415

helps us to understand the biocompatible behavior of materials for wound healing applications.[44] We have conducted different biological assays to evaluate the biological potential of bioactive wound dressing materials for wound healing applications. Figure 8i−ix shows the cell morphology evaluating the cellular behavior against bioactive hydrogels after different intervals (24, 48, and 72 h). Increased contact time increased the cell population with a proper cylindrical shape, as shown in Figure 8i−ix, and negligible or no cell death

was observed, as denoted by a red spot. It is also important to note that these cells from HGel-1 to HGel-3 have mature, cylindrical, and spreading morphologies after 72 h. These led to the mature cell morphology from HGel-1 to HGel-3, which offers a promising microenvironment for cellular activities and its growth.[45]

The cell viability and proliferation have been characterized against different dilutions and contact times using 3T3 cell lines of bioactive hydrogels, as shown in Figure 8. The increased cell viability was observed with increased hydrogel dilutions (after 72 h), as shown in Figure 8Bi−iii. Similar behavior of 3T3 cell lines has been observed for cell proliferation, i.e., increased hydrogel contents and contact time increase cell proliferation and growth, as shown in Figure 8Ci−iii. HGel-3 exhibited maximum cell viability and proliferation, possibly due to the incorporation of GO and gelatin into the crosslinked hydrogel. Both (GO and gelatin) offer a desirable microenvironment, which enhances cell viability and proliferation by offering an additional active site and binding functional groups through different weak forces of attraction, including hydrogen bonding.[46] Hence, the fabricated bioactive hydrogels have offered exceptional cell viability and proliferation that may be potential dressing for wound healing applications.

4.9. Antibacterial Activities. The antibacterial activities of hydrogels were evaluated against infection-causing Gram (positive and negative) bacterial pathogens (*E. coli*, *P. aeruginosa*, and *S. aureus*), as shown in Figure 8D. The hydrogels have different antibacterial activities due to their different structural behaviors, and we have taken curcumin as a positive control. The GO-incorporated hydrogels (HGel-2 and HGel-3) have potential antibacterial activities that could be the synergistic effect of the polymer and GO. It may have electrostatic interaction due to its sp2 hybridization with the
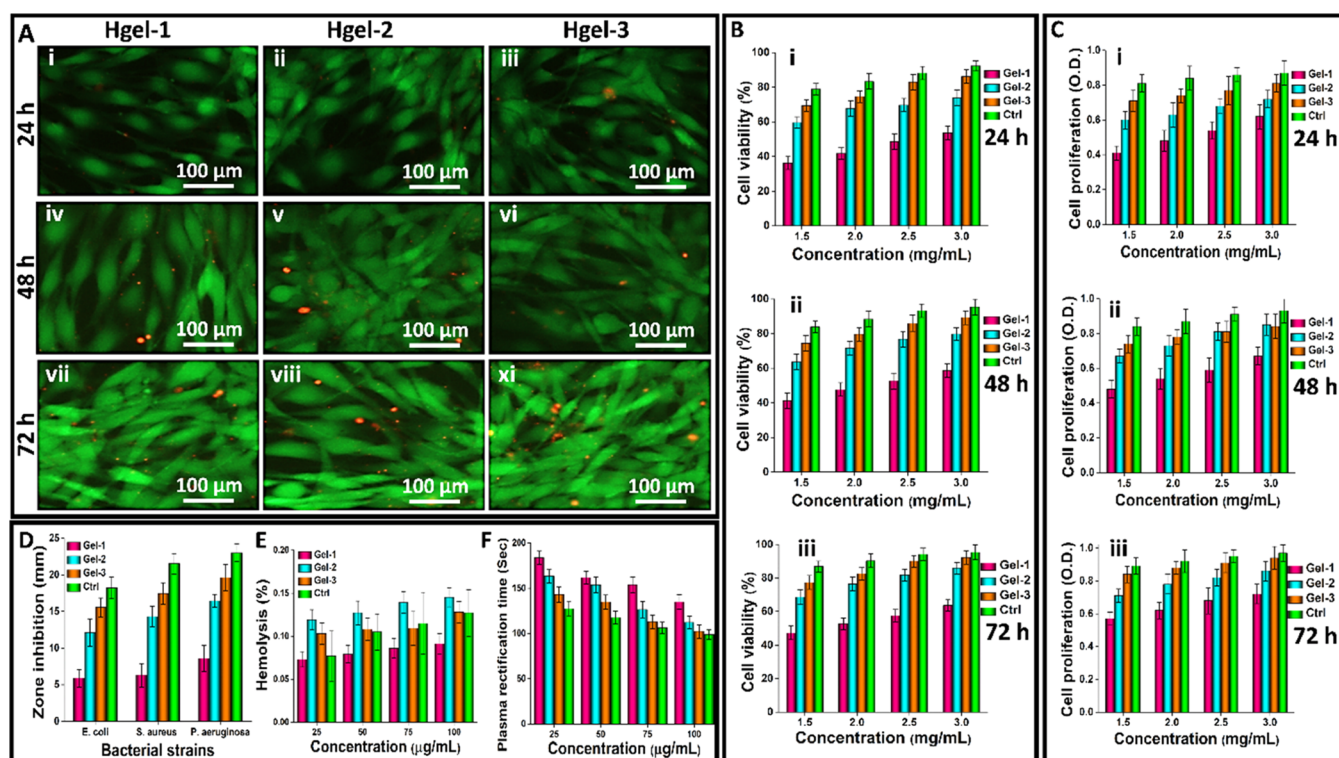
Figure 8. Biological activities were characterized to determine the behavior of bioactive hydrogels against time and different dilutions of bioactive hydrogels using 3T3 cell lines, fresh blood, and infection-causing bacterial strains. The cell morphology A(i−ix) of the 3T3 cell line after different time intervals (48 and 72 h). Cell viability B(i−iii) and cell proliferation C(i−iii) of *3T3* against different dilutions of bioactive hydrogels (1.5−3.0 mg/mL) after different times (24, 48, and 72 h). The increased cell viability was observed by increasing hydrogel contents and contact time and increasing contact time and dilutions of the bioactive hydrogel. The antibacterial activities (D) against different *E. coli*, *P. aeruginosa*, and *S. aureus* via the zone inhibition method and hemocompatibility (E hemolysis (%) and F plasma rectification time (in seconds)) with different hydrogel dilutions.

bacterial membrane, as the outer membrane comprises phospholipids and lipopolysaccharides.[47] GO may adhere to bacterial membranes via electrostatic interactions to produce a twisting effect that may rupture the bacterial membranes to hinder bacterial growth. The polymeric part of hydrogels may interact with bacterial phospholipids and lipopolysaccharides. It may enter a bacterial cell to endorse a charge that controls bacterial growth by preventing translation and transcription.[48] The polymeric part may bind to bacterial DNA that transforms to take control of bacterial cells to inhibit further growth of bacteria, which causes antibacterial activities.[49] These bioactive hydrogels processed substantial antibacterial activities and would be potential antibacterial wound-healing materials for wound healing applications.

4.10. Hemolysis and Blood Coagulation Times. The wound dressing material must interact with blood and be hemocompatible to control bleeding without causing hemotoxicity or hemolysis. While interacting with blood, a small portion of the bioactive hydrogel may enter the body through leaked blood vessels.[50] Therefore, we have performed biocompatibility and hemocompatibility assays against different bioactive hydrogel dilutions to find an optimized formulation, as shown in Figure 8E,F. All bioactive hydrogels have less than 5% hemolysis rate, and all the hydrogel samples with all different dilutions are hemocompatible. Little or negligible hemolysis was observed due to the twisting effect of GO that may electrostatically interact with blood cells, as shown in Figure 8E. The hydrogel without GO has the least hemolysis effect compared to other hydrogels. Hence, the

fabricated bioactive hydrogels are hemocompatible with negligible hemolysis and would be a potential wound-healing material in biomedical applications.

The blood clotting time is another essential component of hemocompatibility; clinically applied wound dressings must have blood clotting properties that prevent bleeding without consequential hemotoxicity. The blood cells may start clotting as they come into contact with a polymeric hydrogel matrix that significantly protects against further bleeding. The bleeding pressure, the size of the wound, and the use of a mechanically stable dressing are all essential factors preventing bleeding.[51] The blood clotting phenomenon, also known as blood coagulation, which produces thrombin from the prothrombin plasma precursor and is known to stop bleeding, has an average blood coagulation time of 1−3 min. However, the production of insoluble fibrin from soluble fibrinogen causes blood to clot. The manufactured wound dressing materials were found to have various blood coagulation times.[52] The blood coagulation time is the fastest in the hydrogel sample (HGel-1) and then slows down in HGel-2 and HGel-3, as shown in Figure 8F. GO plays a vital role in blood coagulation, and hydrogels with a different composition also promote hemocompatibility due to enhanced functional, structural, mechanical, and other morphological features. Hydrogel dilution was also an essential parameter as the least coagulation time was observed at 25 μg/mL with the maximum observed at 100 μg/mL. Hence, the fabricated hydrogels are hemocompatible and offer negligible hemolysis and time coagulation with a response.

5. CONCLUSIONS

The bioactive hydrogels were fabricated for wound healing applications. The graphene oxide-functionalized bacterial cellulose was synthesized using the hydrothermal method and chemically crosslinked with bacterial cellulose and gelatin to produce hydrogels using TEOS as a crosslinker. It was observed that GO-*f*-BC-gelatin hydrogel is more hydrophilic and offers better surface morphology with multifunctional properties due to the presence of gelatin compared to other hydrogels BC-BC and GO-*f*-BC-BC hydrogels. However, these hydrogels have shown different curcumin release behaviors against time under similar conditions, and Hgel-3 has delayed curcumin release. The drug release kinetics was studied against different models from drug release data, and all hydrogels exhibited the Hixson−Crowell model. It was also observed that GO-*f*-BC-gelatin hydrogel had enhanced cell viability and proliferation with mature cell morphology due to its multifunctional behavior. The hydrogel BC-BC has the least hemolysis and antibacterial activities, and all hydrogels are hemocompatible. Hgel-3 has significant antibacterial activities due to the synergistic effects of BG, Gel, and GO. The overall results show that the fabricated hydrogels have multifunctional behavior with different drug release behaviors offering exceptional antibacterial activities, mature morphology, cell viability, proliferation, and hemocompatibility. Hence, these hydrogels would be potential wound dressing materials for wound healing applications.

■ AUTHOR INFORMATION

Corresponding Authors

Muhammad Umar Aslam Khan − *Biomedical Research Center, Qatar University, Doha 2713, Qatar; Department of Mechanical and Industrial Engineering, Qatar University, Doha 2713, Qatar;* ⊙ orcid.org/0000-0001-8105-2651; Email: umar007khan@gmail.com

Roselinda Ab Rehman − *Oral and Maxillofacial Surgery Unit, School of Dental Sciences, Universiti Sains Malaysia, 16150 Kubang Kerian, Kelantan, Malaysia;* Email: roselinda@usm.my

Anwarul Hasan − *Biomedical Research Center, Qatar University, Doha 2713, Qatar; Department of Mechanical and Industrial Engineering, Qatar University, Doha 2713, Qatar;* ⊙ orcid.org/0000-0001-8380-2233; Email: ahasan@qu.edu.qa

Authors

Goran M. Stojanović − *Department of Electronics, Faculty of Technical Sciences, University of Novi Sad, 21000 Novi Sad, Serbia;* ⊙ orcid.org/0000-0003-2098-189X

Ali-Reza Moradi − *Department of Physics, Institute for Advanced Studies in Basic Sciences (IASBS), Zanjan 45137-66731, Iran*

Muhammad Rizwan − *Department of Chemistry, Universiti Malaya, 50603 Kuala Lumpur, Malaysia*

Nureddin Ashammakhi − *Department of Biomedical Engineering and the Institute for Quantitative Health Science & Engineering, Michigan State University, East Lansing, Michigan 48824, United States;* ⊙ orcid.org/0000-0003-0181-6055

Complete contact information is available at:
https://pubs.acs.org/10.1021/acsomega.2c06825

Author Contributions

Conceptualization: M.U.A.K.; data curation: M.U.A.K. and G.M. S.; formal analysis: M.U.A.K., M.R., and A.-R.M.; funding acquisition: M.U.A.K. and G.M.S.; investigation: G.M.S., N.A., and A.H.; methodology: M.U.A.K., R.A.R., and G.M.S.; project administration: M.R. and M.U.A.K.; resources: M.U.A.K., R.A.R., and G.M.S.; software: M.U.A.K., N.A., and M.R.; supervision: R.A.R. and G.M.S.; validation: R.A.R. and A.H.; visualization: M.U.A.K.; writing—original draft: M.U.A.K.; and writing—review and editing: M.U.A.K. and G.M.S and N.A.

Notes

The authors declare no competing financial interest.

■ ACKNOWLEDGMENTS

■ REFERENCES

(1) Chen, G.; Yu, Y.; Wu, X.; Wang, G.; Ren, J.; Zhao, Y. Wound healing: Bioinspired multifunctional hybrid hydrogel promotes wound healing. *Adv. Funct. Mater.* **2018**, *28*, No. 1870233.

(2) Liang, Y.; He, J.; Guo, B. Functional hydrogels as wound dressing to enhance wound healing. *ACS Nano* **2021**, *15*, 12687−12722.

(3) Khan, M. U. A.; Abd Razak, S. I.; Mehboob, H.; Abdul Kadir, M. R.; Anand, T. J. S.; Inam, F.; Shah, S. A.; Abdel-Haliem, M. E.; Amin, R. Synthesis and characterization of silver-coated polymeric scaffolds for bone tissue engineering: antibacterial and in vitro evaluation of cytotoxicity and biocompatibility. *ACS Omega* **2021**, *6*, 4335−4346.

(4) Tu, Z.; Chen, M.; Wang, M.; Shao, Z.; Jiang, X.; Wang, K.; Yao, Z.; Yang, S.; Zhang, X.; Gao, W.; et al. Engineering bioactive M2 macrophage-polarized anti-inflammatory, antioxidant, and antibacterial scaffolds for rapid angiogenesis and diabetic wound repair. *Adv. Funct. Mater.* **2021**, *31*, No. 2100924.

(5) Prasathkumar, M.; Sadhasivam, S. Chitosan/hyaluronic acid/alginate and an assorted polymers loaded with honey, plant, and marine compounds for progressive wound healing—know-how. *Int. J. Biol. Macromol.* **2021**, *186*, 656−685.

(6) Tang, Y.; Zhang, X.; Li, X.; Ma, C.; Chu, X.; Wang, L.; Xu, W. A review on recent advances of Protein-Polymer hydrogels. *Eur. Polym. J.* **2022**, *162*, No. 110881.

(7) Al-Arjan, W. S.; Aslam Khan, M. U.; Nazir, S.; Abd Razak, S. I.; Abdul Kadir, M. R. Development of arabinoxylan-reinforced apple pectin/graphene oxide/nano-hydroxyapatite based nanocomposite scaffolds with controlled release of drug for bone tissue engineering: in-vitro evaluation of biocompatibility and cytotoxicity against MC3T3-E1. *Coatings* **2020**, *10*, 1120.

(8) Shahi, S.; Roghani-Mamaqani, H.; Talebi, S.; Mardani, H. Chemical stimuli-induced reversible bond cleavage in covalently crosslinked hydrogels. *Coord. Chem. Rev.* **2022**, *455*, No. 214368.

(9) Shafiei, M.; Ansari, M. N. M.; Razak, S. I. A.; Khan, M. U. A. A comprehensive review on the applications of exosomes and liposomes in regenerative medicine and tissue engineering. *Polymers* **2021**, *13*, 2529.

(10) Yang, Q.; Hu, Z.; Rogers, J. A. Functional hydrogel interface materials for advanced bioelectronic devices. *Acc. Mater. Res.* **2021**, *2*, 1010−1023.

(11) Manzoor, A.; Dar, A. H.; Pandey, V. K.; Shams, R.; Khan, S.; Panesar, P. S.; Kennedy, J. F.; Fayaz, U.; Khan, S. A. Recent insights into polysaccharide-based hydrogels and their potential applications in food sector: a review. *Int. J. Biol. Macromol.* **2022**, *213*, 987−1006.

(12) Aslam Khan, M. U.; Haider, A.; Abd Razak, S. I.; Abdul Kadir, M. R.; Haider, S.; Shah, S. A.; Hasan, A.; Khan, R.; Khan, S. u. d.; Shakir, I. Arabinoxylan/graphene-oxide/nHAp-NPs/PVA bionano

composite scaffolds for fractured bone healing. *J. Tissue Eng. Regener. Med.* **2021**, *15*, 322−335.

(13) Albuquerque, P. B. S.; de Oliveira, W. F.; dos Santos Silva, P. M.; dos Santos Correia, M. T.; Kennedy, J. F.; Coelho, L. C. B. B. Skincare application of medicinal plant polysaccharides—A review. *Carbohydr. Polym.* **2022**, *277*, No. 118824.

(14) Hasan, A.; Waters, R.; Roula, B.; Dana, R.; Yara, S.; Alexandre, T.; Paul, A. Engineered biomaterials to enhance stem cell-based cardiac tissue engineering and therapy. *Macromol. Biosci.* **2016**, *16*, 958−977.

(15) Li, B.; Kennedy, J.; Jiang, Q.; Xie, B. Quick dissolvable, edible and heatsealable blend films based on konjac glucomannan—gelatin. *Food Res. Int.* **2006**, *39*, 544−549.

(16) Wang, J.; Tang, F.; Wang, Y.; Lu, Q.; Liu, S.; Li, L. Self-healing and highly stretchable gelatin hydrogel for self-powered strain sensor. *ACS Appl. Mater. Interfaces* **2020**, *12*, 1558−1566.

(17) Zamri, M. F. M. A.; Bahru, R.; Amin, R.; Khan, M. U. A.; Abd Razak, S. I.; Hassan, S. A.; Kadir, M. R. A.; Nayan, N. H. M. Waste to health: A review of waste derived materials for tissue engineering. *J. Cleaner Prod.* **2021**, *290*, No. 125792.

(18) Zhou, K.; Zhang, Z.; Xue, J.; Shang, J.; Ding, D.; Zhang, W.; Liu, Z.; Yan, F.; Cheng, N. Hybrid Ag nanoparticles/polyoxometalate-polydopamine nano-flowers loaded chitosan/gelatin hydrogel scaffolds with synergistic photothermal/chemodynamic/Ag+ anti-bacterial action for accelerated wound healing. *Int. J. Biol. Macromol.* **2022**, *221*, 135−148.

(19) Khan, M. U. A.; Haider, S.; Raza, M. A.; Shah, S. A.; Abd Razak, S. I.; Kadir, M. R. A.; Subhan, F.; Haider, A. Smart and pH-sensitive rGO/Arabinoxylan/chitosan composite for wound dressing: In-vitro drug delivery, antibacterial activity, and biological activities. *Int. J. Biol. Macromol.* **2021**, *192*, 820−831.

(20) Depan, D.; Girase, B.; Shah, J.; Misra, R. D. K. Structure—process—property relationship of the polar graphene oxide-mediated cellular response and stimulated growth of osteoblasts on hybrid chitosan network structure nanocomposite scaffolds. *Acta Biomater.* **2011**, *7*, 3432−3445.

(21) Abadi, A. J.; Mirzaei, S.; Mahabady, M. K.; Hashemi, F.; Zabolian, A.; Hashemi, F.; Raee, P.; Aghamiri, S.; Ashrafizadeh, M.; Aref, A. R.; et al. Curcumin and its derivatives in cancer therapy: Potentiating antitumor activity of cisplatin and reducing side effects. *Phytother. Res.* **2022**, *36*, 189−213.

(22) Abd El-Hack, M. E.; El-Saadony, M. T.; Swelum, A. A.; Arif, M.; Abo Ghanima, M. M.; Shukry, M.; Noreldin, A.; Taha, A. E.; El-Tarabily, K. A. Curcumin, the active substance of turmeric: its effects on health and ways to improve its bioavailability. *J. Sci. Food Agric.* **2021**, *101*, 5747−5762.

(23) Ghosal, K.; Augustine, R.; Zaszczynska, A.; Barman, M.; Jain, A.; Hasan, A.; Kalarikkal, N.; Sajkiewicz, P.; Thomas, S. Novel drug delivery systems based on triaxial electrospinning based nanofibers. *React. Funct. Polym.* **2021**, *163*, No. 104895.

(24) Abba, M.; Ibrahim, Z.; Chong, C. S.; Zawawi, N. A.; Kadir, M. R. A.; Yusof, A. H. M.; Razak, S. I. A. Transdermal delivery of crocin using bacterial nanocellulose membrane. *Fibers Polym.* **2019**, *20*, 2025−2031.

(25) Nazir, S.; Khan, M. U. A.; Al-Arjan, W. S.; Abd Razak, S. I.; Javed, A.; Kadir, M. R. A. Nanocomposite hydrogels for melanoma skin cancer care and treatment: In-vitro drug delivery, drug release kinetics and anti-cancer activities. *Arabian J. Chem.* **2021**, *14*, No. 103120.

(26) Khan, M. U. A.; Razak, S. I. A.; Ansari, M. N. M.; Zulkifli, R. M.; Ahmad Zawawi, N.; Arshad, M. Development of biodegradable bio-based composite for bone tissue engineering: synthesis, characterization and in vitro biocompatible evaluation. *Polymers* **2021**, *13*, 3611.

(27) Suhag, A.; Biswas, K.; Singh, S.; Kulshreshtha, A. Crosslinking effect on polyvinyl alcohol resin for barrier properties of barrier biaxial orientation films. *Prog. Org. Coat.* **2022**, *163*, No. 106662.

(28) Al-Arjan, W. S.; Khan, M. U. A.; Almutairi, H. H.; Alharbi, S. M.; Razak, S. I. A. pH-Responsive PVA/BC-f-GO Dressing Materials

for Burn and Chronic Wound Healing with Curcumin Release Kinetics. *Polymers* **2022**, *14*, 1949.

(29) Sudhakar, K.; Suneetha, M.; Rao, K. M.; Han, S. S. Antibacterial reduced graphene oxide reinforces polyelectrolyte hydrogels with polysaccharides via a green method. *Colloids Surf., A* **2021**, *628*, No. 127340.

(30) Feng, Z.; Zuo, H.; Hu, J.; Gao, W.; Yu, B.; Ning, N.; Tian, M.; Zhang, L. Mussel-inspired highly stretchable, tough nanocomposite hydrogel with self-healable and near-infrared actuated performance. *Ind. Eng. Chem. Res.* **2020**, *59*, 166−174.

(31) Khan, M. U. A.; Iqbal, I.; Ansari, M. N. M.; Razak, S. I. A.; Raza, M. A.; Sajjad, A.; Jabeen, F.; Riduan Mohamad, M.; Jusoh, N. Development of antibacterial, degradable and ph-responsive chitosan/guar gum/polyvinyl alcohol blended hydrogels for wound dressing. *Molecules* **2021**, *26*, 5937.

(32) Khan, S.; Khan, M. U.; Ullah, Z.Drying: A Versatile Fabrication of Porous Biomaterials *Biomater. Fabr. Tech.* 2022, p 46.

(33) Amagat, J.; Su, Y.; Svejsø, F. H.; Le Friec, A.; Sønderskov, S. M.; Dong, M.; Fang, Y.; Chen, M. Self-snapping hydrogel-based electroactive microchannels as nerve guidance conduits. *Mater. Today Bio* **2022**, *16*, No. 100437.

(34) Douglass, M.; Garren, M.; Devine, R.; Mondal, A.; Handa, H. Bio-inspired hemocompatible surface modifications for biomedical applications. *Prog. Mater. Sci.* **2022**, *130*, No. 100997.

(35) Khan, M. U.; Stojanović, G. M.; Hassan, R.; Anand, T. J.; Al-Ejji, M.; Hasan, A. Role of graphene oxide in bacterial cellulose—gelatin hydrogels for wound dressing applications. *ACS Omega* **2023**, *8*, 15909−15919.

(36) Du, C.; Zhang, X. N.; Sun, T. L.; Du, M.; Zheng, Q.; Wu, Z. L. Hydrogen-bond association-mediated dynamics and viscoelastic properties of tough supramolecular hydrogels. *Macromolecules* **2021**, *54*, 4313−4325.

(37) Qian, C.; Zhang, T.; Gravesande, J.; Baysah, C.; Song, X.; Xing, J. Injectable and self-healing polysaccharide-based hydrogel for pH-responsive drug release. *Int. J. Biol. Macromol.* **2019**, *123*, 140−148.

(38) Liu, B.; Zhu, H.; Zhao, D.; Nian, G.; Qu, S.; Yang, W. Hydrogel coating enabling mechanically friendly, step-index, functionalized optical fiber. *Adv. Opt. Mater.* **2021**, *9*, No. 2101036.

(39) Zeng, N.; He, L.; Jiang, L.; Shan, S.; Su, H. Synthesis of magnetic/pH dual responsive dextran hydrogels as stimuli-sensitive drug carriers. *Carbohydr. Res.* **2022**, *520*, No. 108632.

(40) De Piano, R.; Caccavo, D.; Cascone, S.; Festa, C.; Lamberti, G.; Barba, A. A. Drug release from hydrogel-based matrix systems partially coated: Experiments and modeling. *J. Drug Delivery Sci. Technol.* **2021**, *61*, No. 102146.

(41) Emam, H. E.; Shaheen, T. I. Design of a dual pH and temperature responsive hydrogel based on esterified cellulose nanocrystals for potential drug release. *Carbohydr. Polym.* **2022**, *278*, No. 118925.

(42) Herdiana, Y.; Wathoni, N.; Shamsuddin, S.; Muchtaridi, M. Drug release study of the chitosan-based nanoparticles. *Heliyon* **2022**, *8*, No. e08674.

(43) Jafari, S.; Soleimani, M.; Badinezhad, M. Application of different mathematical models for further investigation of in vitro drug release mechanisms based on magnetic nano-composite. *Polymer Bull.* **2022**, *79*, 1021−1038.

(44) Somasekharan, L. T.; Raju, R.; Kumar, S.; Geevarghese, R.; Nair, R. P.; Kasoju, N.; Bhatt, A. Biofabrication of skin tissue constructs using alginate, gelatin and diethylaminoethyl cellulose bioink. *Int. J. Biol. Macromol.* **2021**, *189*, 398−409.

(45) Luo, Y.; Wei, X.; Huang, P. 3D bioprinting of hydrogel-based biomimetic microenvironments. *J. Biomed. Mater. Res., Part B* **2019**, *107*, 1695−1705.

(46) Erkoc, P.; Uvak, I.; Nazeer, M. A.; Batool, S. R.; Odeh, Y. N.; Akdogan, O.; Kizilel, S. 3D printing of cytocompatible gelatin-cellulose-alginate blend hydrogels. *Macromol. Biosci.* **2020**, *20*, No. 2000106.

(47) Wei, P.; Wang, L.; Xie, F.; Cai, J. Strong and tough cellulose—graphene oxide composite hydrogels by multi-modulus components

strategy as photothermal antibacterial platform. *Chem. Eng. J.* **2022**, *431*, No. 133964.

(48) Nikfarjam, N.; Ghomi, M.; Agarwal, T.; Hassanpour, M.; Sharifi, E.; Khorsandi, D.; Ali Khan, M.; Rossi, F.; Rossetti, A.; Nazarzadeh Zare, E.; et al. Antimicrobial ionic liquid-based materials for biomedical applications. *Adv. Funct. Mater.* **2021**, *31*, No. 2104148.

(49) Mao, L.; Wang, L.; Zhang, M.; Ullah, M. W.; Liu, L.; Zhao, W.; Li, Y.; Ahmed, A. A. Q.; Cheng, H.; Shi, Z.; Yang, G. In situ synthesized selenium nanoparticles-decorated bacterial cellulose/gelatin hydrogel with enhanced antibacterial, antioxidant, and anti-inflammatory capabilities for facilitating skin wound healing. *Adv. Healthcare Mater.* **2021**, *10*, No. 2100402.

(50) Zhang, F.; Hu, C.; Yang, L.; Liu, K.; Ge, Y.; Wei, Y.; Wang, J.; Luo, R.; Wang, Y. A conformally adapted all-in-one hydrogel coating: towards robust hemocompatibility and bactericidal activity. *J. Mater. Chem. B* **2021**, *9*, 2697−2708.

(51) Jin, J.; Ji, Z.; Xu, M.; Liu, C.; Ye, X.; Zhang, W.; Li, S.; Wang, D.; Zhang, W.; Chen, J.; et al. Microspheres of carboxymethyl chitosan, sodium alginate, and collagen as a hemostatic agent in vivo. *ACS Biomater. Sci. Eng.* **2018**, *4*, 2541−2551.

(52) Khan, M. U. A.; Razaq, S. I. A.; Mehboob, H.; Rehman, S.; Al-Arjan, W. S.; Amin, R. Antibacterial and hemocompatible pH-responsive hydrogel for skin wound healing application: In vitro drug release. *Polymers* **2021**, *13*, 3703.